Theoretical study of figure-eight all-fiber laser

Mohamed Salhi, Adil Haboucha, Hervé Leblond, François Sanchez

Theoretical study of figure-eight all-fiber laser

M. Salhi, A. Haboucha, H. Leblond, and F. Sanchez
Laboratoire POMA, CNRS-FRE 2988, Université d'Angers, 2 Boulevard Lavoisier, 49000 Angers, France
(Received 10 October 2007; published 13 March 2008)

We report a fully analytical study of figure-eight passively mode-locked fiber lasers. An adapted master equation is established for the figure-eight fiber laser. It is of cubic complex Ginzburg-Landau type, in which the coefficients explicitly depend on the characteristics of the cavity. We derive stability conditions for passively mode-locked and continuous wave operations in both net positive dispersion and net negative dispersion. In the soliton regime, the duration and the pulse energy are studied. The model points out a great sensitivity of pulse characteristics on parameters of the cavity, in particular, on the orientation of the polarizing isolator, on the coupling coefficient of the fiber coupler and on the length of the nonlinear optical loop mirror.

DOI: 10.1103/PhysRevA.77.033828 PACS number(s): 42.55.Wd

I. INTRODUCTION

Mode-locked regime, generated by passive techniques in fiber lasers, has been extensively investigated both experimentally and theoretically. Passive techniques are very attractive because they are able to easily produce self-starting ultrashort pulses. The first methods proposed for passive mode-locking utilized saturable absorbers. The latter create high losses in wings and weak attenuation in the central part of a pulse leading to the formation of ultrashort pulses. The principle of the methods often exploit nonlinear effects induced by self-phase and cross-phase modulation, both resulting from the optical Kerr effect. Additive pulse mode locking [1] has also been used to generate ultrashort pulses. The laser is formed by two cavities coupled by a common mirror. The first one, called the laser cavity, contains the gain medium while the second one, called the auxiliary cavity, introduces intensity-dependent losses. An artificial saturable absorber is therefore created in the laser allowing the emergence of a pulsed regime. The nonlinear polarization rotation technique, developed by Matsas [2], is a powerful tool for the generation of femtosecond pulses. The laser configuration consists in a fiber ring cavity containing two polarization controllers placed at each side of a polarizer. If the polarization controllers are suitably oriented, the polarizer lets pass the central intense part of a pulse, while it blocks the low intensity wings. Among the different techniques available, figure-eight mode locking has been one of the most influential to date, resulting in pulses as short as 125 fs [3]. Two configurations can be used to achieve stable pulses. The first one consists of a nonlinear amplifying loop mirror (NALM), containing an optical isolator, coupled with a nonlinear optical loop mirror (NOLM) through an asymmetrical fiber coupler. In this case, the pulse operation in the laser is due to the intensity-dependent reflectivity of the NOLM. In the second design, the NALM and NOLM are coupled by a symmetrical coupler and the isolator is inserted in the NOLM. The NALM creates an artificial saturable absorber.

Numerous experimental results have been reported demonstrating the generation of subpicosecond pulses by the figure eight configuration. Guy *et al.* [4] reported pulses as short as 620 fs pulse at 1.3 μm in a praseodymium fluoride fiber laser. A pulse duration of 700 fs with spectrum bandwidth of 14 nm has been obtained in erbium doped fiber [5]. 850 fs mode-locked pulse at 1065 nm is reported in Ref. [6] using a totally fiber integrated figure eight laser. Zhao *et al.* [7] have reported the realization of high-power figure eight laser with passive subring loops for repetition rate control. From the theoretical point of view, different models have been developed. Numerical simulations, reported by Theimer and Haus [8], demonstrated that the pulse width depends on several factors including the amplifier gain and length, and the length of the NOLM. However, to the best of our knowledge, all the theoretical approaches require numerical simulations because there is no analytic solutions to the master equation. In addition, the master equation used is not related to the exact details of the optical configuration but it is rather the result of a phenomenological approach.

The aim of this paper is to provide an analytical analysis of the figure-eight laser. In particular, it is of great importance to study the stability of the mode-locking solution. Based on our previous works concerning passively mode-locked fiber lasers with nonlinear polarization rotation [9–11], we will determine a master equation for the figure-eight fiber laser. The resulting model reduces to a cubic complex Ginzburg-Landau (CGL) equation which admits analytical stationary and localized solutions. Stability condition can be found for both solutions. The paper is organized as follows. Section II is devoted to the normal dispersion regime. It is first derived the master equation for the electric field amplitude. The final equation takes into account explicitly the physical parameters of the optical cavity, such as the orientation of the polarizer and the coupling coefficient of the fiber coupler. cw (continuous wave) and mode-lock solutions are found and their stability is investigated. The anomalous dispersion case is considered in Sec. III. In this case, it is possible to calculate the energy and the duration of the pulses.

Before to proceed, let us specify the exact optical configuration which will be considered in this paper. The setup is schematically represented in Fig. 1, it consists in coupled NALM and NOLM. The coupling is provided by a fiber coupler with a coupling coefficient k considered as a variable parameter. The NALM is formed by a wavelength-division multiplexer (WDM) used to launch the pump power into the fiber laser cavity, a polarizing isolator, a piece of a standard fiber of length $L_1=1$ m placed between the isolator and the

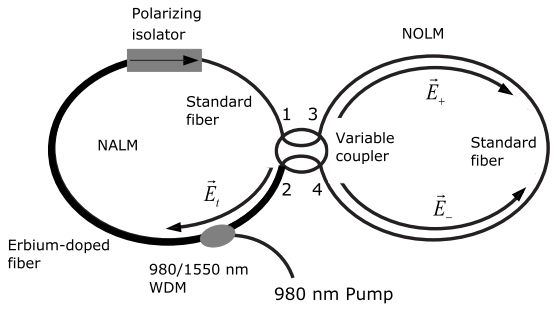

FIG. 1. Configuration of a figure-eight fiber laser.

coupler, and an erbium doped fiber characterized by the following parameters: length $L_{\mathrm{Er}}=10$ m, group-velocity dispersion (GVD) $\beta_2^{\mathrm{Er}}=0.075$ ps^2 m^{-1}, a nonlinear coefficient $\gamma=0.002$ W^{-1} m^{-1} and birefringent parameter $n_{\mathrm{Er}}=0.1$ m^{-1}. The output coupling is provided by a coupler placed just after the polarizing isolator (it is not represented in the figure and, in the following, it will be included in the polarizer through a transmission which will be less than unity). The NOLM contain a variable length L_2 of standard fiber characterized by the following parameters: GVD $\beta_2^s=-0.022$ ps^2 m^{-1}, nonlinear coefficient $\gamma=0.002$ W^{-1} m^{-1} and birefringent parameter $n_s=1$ m^{-1}.

II. NORMAL DISPERSION

In this section we consider the case of net positive dispersion, i.e., $\eta=\beta_2^s(L_1+L_2)+\beta_2^{\mathrm{Er}}L_{\mathrm{Er}}>0$. This situation occurs when the length of the NOLM is less than 33 m. The total cavity dispersion η is negative for $L_2>33$ m. Our goal is first to derive a master equation for the laser shown in Fig. 1. For that, the fully vectorial equations of the electric field amplitude are solved in the different fibers using the procedure that we developed in Ref. [9]. A perturbation expansion yields analytic expressions. The electric field is considered at the exit of the polarizer where it is a scalar quantity because it has a well-defined linear polarization. This allows us to obtain a relation of the electric field at the $(n+1)$th round-trip as a function of its amplitude at the nth round-trip. The discrete sequence can be transformed in a continuous equation which is of CGL type. The important point in our analysis is that the coefficients of the equation explicitly depend on all parameters of the fiber laser cavity. Finally, the CGL equation admits analytic solutions allowing to perform a stability analysis.

A. Propagation of light inside the cavity

1. Propagation along the standard fiber

The complex amplitude of the electric field is decomposed into two polarization components (u and v). Each component evolves nonlinearly in the fiber and undergoes GVD and birefringence. In the frame moving at the group velocity, the system is described by two coupled nonlinear Schrödinger equations [9,12]:

$$i\frac{\partial u}{\partial z}-n_s u-\frac{\beta_2^s}{2}\frac{\partial^2 u}{\partial t^2}+\gamma(u|u|^2+A|v|^2+Bv^2u^*)=0, \quad (1)$$

$$i\frac{\partial v}{\partial z}+n_s v-\frac{\beta_2^s}{2}\frac{\partial^2 v}{\partial t^2}+\gamma(v|v|^2+A|u|^2+Bu^2v^*)=0, \quad (2)$$

where A and B are the dielectric coefficients. In isotropic media, $A=2/3$ and $B=1/3$ [12].

Following the approach given in Refs. [9–11], we assume that the GVD β_2^s and the nonlinear coefficient γ are small quantities (of order ϵ) and we use a first-order perturbative approach. Equations (1) and (2) lead to approximate analytic expressions relating the electric-field components $[u(L_1),v(L_1)]$ at the exit of the piece of the standard fiber of length L_1 to the ones at its entrance $[u(0),v(0)]$. These explicit expressions are given in the Appendix.

2. The fiber coupler and the NOLM

The electric-field $[u(L_1),v(L_1)]$ is divided by the coupler into two counterpropagating fields noted $\vec{E}_{\pm}$ in the fiber loop, where $\vec{E}_+=\sqrt{k}(u(L_1),v(L_1))$ and $\vec{E}_-=i\sqrt{1-k}(u(L_1),v(L_1))$, with k as the coupling coefficient. It is important to note that, for short pulses, the two waves cross in a very short distance compared to the fiber loop length (for example for 10 ps pulses, the crossing spreads over 2 mm). Therefore it is possible to neglect the cross-phase modulation between the two counterpropagating fields. This allowed us to analytically solve the problem in the stationary regime [13].

The evolution of $\vec{E}_{\pm}$ is governed by equations similar to Eqs. (1) and (2). Under the same approximations, the system is solved and, after propagation over the length L_2, we get expressions of $E_{\pm u}(L_2)$ and $E_{\pm v}(L_2)$, given in the Appendix.

The transmitted field by the NOLM result from the recombination at the exit of the coupler of two counterpropagating waves after a round-trip in a loop of length L_2. It is given by

$$\vec{E}_t=\begin{pmatrix}E_{tu}\\E_{tv}\end{pmatrix}=\sqrt{k}\begin{pmatrix}E_{+u}(L_2)\\E_{+v}(L_2)\end{pmatrix}+i\sqrt{1-k}\begin{pmatrix}E_{-u}(L_2)\\E_{-v}(L_2)\end{pmatrix}. \quad (3)$$

3. Propagation along the erbium-doped fiber

We describe here the propagation of the transmitted field $\vec{E}_t$ along the erbium-doped fiber. $\vec{E}_t$ is affected not only by the optical Kerr effect and the dispersion but it also undergoes amplification by the active medium.

The nonlinear evolution of $\vec{E}_t$ is governed by [9,11,12,14]

$$i\frac{\partial E_{tu}}{\partial z}-n_{\mathrm{Er}}E_{tu}-\frac{\beta_2^{\mathrm{Er}}}{2}\frac{\partial^2 E_{tu}}{\partial t^2}+\gamma(E_{tu}|E_{tu}|^2+AE_{tu}|E_{tv}|^2+BE_{tv}^2E_{tu}^*)=ig\left(1+\frac{1}{\omega_g^2}\frac{\partial^2}{\partial t^2}\right)E_{tu}, \quad (4)$$

$$i\frac{\partial E_{tv}}{\partial z} + n_{\mathrm{Er}}E_{tv} - \frac{\beta_2^{\mathrm{Er}}}{2}\frac{\partial^2 E_{tv}}{\partial t^2} + \gamma(E_{tv}|E_{tv}|^2 + AE_{tv}|E_{tu}|^2 + BE_{tu}^2E_{tv}^*) = ig\left(1 + \frac{1}{\omega_g^2}\frac{\partial^2}{\partial t^2}\right)E_{tv}, \tag{5}$$

where $\omega_g = 15.7\ \mathrm{ps}^{-1}$ is the spectral gain bandwidth and g the gain.

As above the solutions of system (4) and (5) are obtained by replacing the quantities β^{Er}, γ and the gain filtering $\rho = g/\omega_g^2$ by $\epsilon\beta^{\mathrm{Er}}$, $\epsilon\gamma$, and $\epsilon\rho$ and by using a perturbative approach. A first order calculation leads to the expressions (A7) and (A8) given in the Appendix.

4. The polarizer

In our model the polarizing isolator plays an important role. First, it allows us to obtain scalar discrete evolution equation for the electric field. In addition it stops the counterpropagating wave in the NALM.

We use the Jones matrix formalism to model the effect of the polarizer on the electric field. We assume that the eigenaxis of the fiber ends, at each side of the polarizing isolator, are aligned and parallel to the x and y axis of the laboratory frame. Let θ be the angle between the passing axis of the polarizer and the x axis. The Jones matrix of the polarizer in the (Ox, Oy) frame can be written as

$$M = \beta\begin{pmatrix} \cos^2\theta & \cos\theta\sin\theta \\ \cos\theta\sin\theta & \sin^2\theta \end{pmatrix}, \tag{6}$$

where $\beta = 95\%$ is the amplitude transmission coefficient of the polarizer.

The electric field after the polarizer is linearly polarized with a polarization parallel to the passing axis of the polarizer. After the nth round-trip, the electric field components at the entrance of the fiber are

$$\begin{pmatrix} u_n(0) \\ v_n(0) \end{pmatrix} = \begin{pmatrix} \cos\theta \\ \sin\theta \end{pmatrix} f_n, \tag{7}$$

where f_n is the electric field amplitude after the nth round-trip evaluated just after the polarizer.

The electric field after the $(n+1)$th round-trip, just after the polarizer, expresses as a function of the electric field components at the nth round-trip $[E_{tu,n}(L_{\mathrm{Er}}), E_{tv,n}(L_{\mathrm{Er}})]$ at the exit of the doped fiber and of the Jones matrix of the polarizer as

$$\begin{pmatrix} \cos\theta \\ \sin\theta \end{pmatrix} f_{n+1} = M\begin{pmatrix} E_{tu,n}(L_{\mathrm{Er}}) \\ E_{tv,n}(L_{\mathrm{Er}}) \end{pmatrix}. \tag{8}$$

B. A master equation for the figure-eight laser

Let us start from the Eq. (8) where we replace $[E_{tu,n}(L_{\mathrm{Er}}), E_{tv,n}(L_{\mathrm{Er}})]$ by their expressions (A7) and (A8). We further replace $(E_{tu,n}, E_{tv,n})$ by the formulas given in Eq. (3). We also take into account the solutions (A3)–(A6) of the components of the two counterpropagating fields after propagation over the length L_2 in the loop. Finally, we introduce the Eqs. (A1) and (A2), and $[u_n(0), v_n(0)]$ is replaced by Eq. (7). After some long and cumbersome algebra we obtain

$$f_{n+1} = \beta e^{gL_{\mathrm{Er}}}Qf_n + \epsilon\beta e^{gL_{\mathrm{Er}}}\left[\left(\chi - \frac{i}{2}\eta\right)Q\frac{\partial^2 f_n}{\partial t^2} + iPf_n|f_n|^2\right] + O(\epsilon^2), \tag{9}$$

where $\chi = \rho L_{\mathrm{Er}}$, $\eta = \beta_2^s(L_1 + L_2) + \beta_2^{\mathrm{Er}}L_{\mathrm{Er}}$ is the net dispersion and

$$Q = (2k-1)[e^{-in_s(L_1+L_2)-in_{\mathrm{Er}}L_{\mathrm{Er}}}\cos^2\theta + e^{in_s(L_1+L_2)+in_{\mathrm{Er}}L_{\mathrm{Er}}}\sin^2\theta], \tag{10}$$

$$P = 2\,\mathrm{Re}[\psi] + 2A(\sigma\,\mathrm{Re}[\varphi e^{-2iL_2n_s}] + \mathrm{Re}[\varphi])\sin^2\theta\cos^2\theta + \varphi(\sigma e^{2iL_2n_s} + 1)\sin^4\theta + \varphi^*(\sigma e^{-2iL_2n_s} + 1)\cos^4\theta + \mu(e^{-2i(L_1+L_2)n_s + iL_{\mathrm{Er}}n_{\mathrm{Er}}} + e^{-iL_{\mathrm{Er}}n_{\mathrm{Er}}}), \tag{11}$$

with

$$\sigma = \frac{(2k-1)^2(e^{2gL_{\mathrm{Er}}} - 1)}{2g(L_1 + L_2)}, \tag{12}$$

$$\psi = \frac{B\gamma(2k-1)^3e^{-i(3L_1+L_2)n_s + iL_{\mathrm{Er}}n_{\mathrm{Er}}}(e^{2L_{\mathrm{Er}}(g-2in_{\mathrm{Er}})} - 1)}{2g - 4in_{\mathrm{Er}}} \times\sin^2\theta\cos^2\theta, \tag{13}$$

$$\varphi = \gamma(2k-1)(L_1 + L_2)e^{i(L_1+L_2)n_s + iL_{\mathrm{Er}}n_{\mathrm{Er}}}, \tag{14}$$

$$\mu = \gamma B(2k-1)\frac{(e^{3i(L_1+L_2)n_s} - e^{-i(L_1+L_2)n_s})}{4in_s}\sin^2\theta\cos^2\theta. \tag{15}$$

It is important to notice that parameters Q and P depend, in particular, on the coupling coefficient k of the fiber coupler, on the orientation θ of the polarizer and on the length L_2 of the NOLM.

By using Eq. (9) it is possible to determine the gain threshold g_0. The expression of the gain is written $g = g_0 + \epsilon g_1$, where g_1 is self-adjusted and corresponds to the excess of the linear gain [9]. The stationary regime is reached when $|f_{n+1}| = |f_n|$, at the order of ϵ^0 this condition gives the expression of g_0, as

$$g_0 = \frac{-1}{2L_{\mathrm{Er}}}\ln(\beta^2|Q|^2) = \frac{-1}{2L_{\mathrm{Er}}}\ln(\beta^2(2k-1)^2\{\cos^4\theta + 2\cos[2(L_1 + L_2)n_s + 2L_{\mathrm{Er}}n_{\mathrm{Er}}]\cos^2\theta\sin^2\theta + \sin^4\theta\}). \tag{16}$$

g_0 is the gain which compensates the linear losses of the laser cavity.

Equation (16) ensures that $|\beta e^{g_0L_{\mathrm{Er}}}Q| = 1$. Denoting the quantity $\beta e^{g_0L_{\mathrm{Er}}}Q$ by $e^{i\alpha}$ and applying a Taylor expansion to $e^{\epsilon g_1L_{\mathrm{Er}}}$, we find the equation

$$f_{n+1} = e^{i\alpha}(1 + \epsilon g_1 L_{\mathrm{Er}}) f_n + \epsilon\left(\chi - \frac{i}{2}\eta\right) e^{i\alpha}\frac{\partial^2 f_n}{\partial t^2} + i\epsilon\frac{e^{i\alpha}}{Q} P f_n |f_n|^2 + O(\epsilon^2). \tag{17}$$

To study the evolution of the field amplitude, it is more convenient to describe it by a continuous equation. The continuous approximation is relevant when the number of round trips is very large, further, mode-locked pulses formation in the cavity requires typically one hundred round trips, i.e., $n \geq 100$. The discrete sequence f_n is interpolated by a continuous function [9] and we obtain

$$i\frac{\partial f}{\partial z} = \frac{-\alpha - i\ln(2k-1)}{L_1 + L_2 + L_{\mathrm{Er}}} f + i\epsilon\frac{g_1 L_{\mathrm{Er}}}{L_1 + L_2 + L_{\mathrm{Er}}} f + \epsilon\left[\frac{\eta/2 + i\chi}{L_1 + L_2 + L_{\mathrm{Er}}}\right]\frac{\partial^2 f}{\partial t^2} + \epsilon\mathcal{D} f |f|^2, \tag{18}$$

where $z = n(L_1 + L_2 + L_{\mathrm{Er}})$ is the longitudinal variable and

$$\mathcal{D} = \frac{-P}{Q[L_1 + L_2 + (2k-1)^2 L_{\mathrm{Er}}]}. \tag{19}$$

At leading order, the solution of Eq. (18) for $k \neq 0.5$ is

$$f = F \exp\left[\frac{-iz\alpha + z\ln(2k-1)}{L_1 + L_2 + L_{\mathrm{Er}}}\right] + O(\epsilon), \tag{20}$$

According to the multiscale analysis [15], we introduce a slow variable $\xi = \epsilon z$. The values of ξ about 1 correspond to number of round trips about L_0/ϵ, with $L_0 = L_1 + L_2 + L_{\mathrm{Er}}$. The knowledge of the small correction $O(\epsilon)$ in Eq. (20) on finite propagation distances z is equivalent to the knowledge of the evolution of the leading amplitude F on very large propagation distances $z \propto L_0/\epsilon$, i.e., $(n \propto 1/\epsilon)$. Setting apart a fast rotating phase factor [9,10], we obtain the cubic complex Ginzburg-Landau (CGL) equation

$$i\frac{\partial F}{\partial \xi} = i\frac{g_1 L_{\mathrm{Er}}}{L_1 + L_2 + L_{\mathrm{Er}}} F + \left[\frac{\eta/2 + i\chi}{L_1 + L_2 + L_{\mathrm{Er}}}\right]\frac{\partial^2 F}{\partial t^2} + (\mathcal{D}_r + i\mathcal{D}_i) F |F|^2, \tag{21}$$

for $k = 0.5$ the parameter Q vanishes. Therefore the threshold gain value g_0 is infinite according to Eq. (16). This is because, any input power to the NOLM is totally reflected and no light is transmitted to the doped fiber. The NOLM acts as a perfect mirror [16]. The isolator inserted in the NALM blocks any counterpropagating wave. The result is that the loss of the cavity is infinite. $\mathcal{D}_r$ is the real part of the quantity $\mathcal{D}$ and corresponds to the effective self-phase modulation. It is always negative. $\mathcal{D}_i$ is the imaginary parts of $\mathcal{D}$ and corresponds to the effective nonlinear gain or absorption.

C. Solutions of the master equation

In this section, we are interested in two particular solutions of Eq. (21). We first investigate the stationary solution corresponding to a continuous wave (cw) operating regime of the laser. Then we study the localized solution. When stable, the latter corresponds to the mode-locking regime of the laser.

1. Stationary solution and its stability

The solution of Eq. (21) with constant and uniform modulus is

$$F = \Gamma e^{i(\kappa\xi - \Omega t)}, \tag{22}$$

where

$$\Omega^2 = \frac{(L_1 + L_2 + L_{\mathrm{Er}})\mathcal{D}_i |\Gamma|^2 + g_1 L_{\mathrm{Er}}}{\chi}, \tag{23}$$

$$\kappa = \frac{\eta}{2\chi}\left(\mathcal{D}_i |\Gamma|^2 + \frac{g_1 L_{\mathrm{Er}}}{(L_1 + L_2 + L_{\mathrm{Er}})}\right) - \mathcal{D}_r |\Gamma|^2. \tag{24}$$

Since Ω represents a mere shift in the carrier frequency, we can set $\Omega = 0$ without loss of generality. Under this condition, the expressions of Γ and κ are

$$\Gamma = \sqrt{\frac{-g_1 L_{\mathrm{Er}}}{\mathcal{D}_i (L_1 + L_2 + L_{\mathrm{Er}})}}, \quad \kappa = \frac{g_1 \mathcal{D}_r L_{\mathrm{Er}}}{\mathcal{D}_i (L_1 + L_2 + L_{\mathrm{Er}})}. \tag{25}$$

Through the expression of Γ we deduce that the constant solution exists only if the product $\mathcal{D}_i g_1$ is negative. In addition, the modulational instability occurs when the excess of linear gain g_1 is negative and the nonlinear gain $\mathcal{D}_i$ is positive [9]. Consequently, the constant amplitude solution is stable when the excess of linear gain is positive and the effective nonlinear gain $\mathcal{D}_i$ is negative.

2. Localized solution and its stability

The localized analytical solution of the Eq. (21) is [17]

$$F = a(t)^{1+id_+} e^{-i\omega_+ \xi}, \tag{26}$$

where the chirp parameter d_+ is

$$d_+ = \frac{-3[\eta\mathcal{D}_r + 2\chi\mathcal{D}_i] + \sqrt{9[2\chi\mathcal{D}_i + \eta\mathcal{D}_r]^2 + 8[\eta\mathcal{D}_i - 2\chi\mathcal{D}_r]^2}}{2[\eta\mathcal{D}_i - 2\chi\mathcal{D}_r]} \tag{27}$$

and

$$\omega_+ = \frac{-g_1 L_{\mathrm{Er}}[4\chi d_+ + \eta d_+^2 - \eta]}{2(L_1 + L_2 + L_{\mathrm{Er}})[\eta d_+^2 - \chi - \eta d_+]}. \tag{28}$$

The real amplitude $a(t)$ is

$$a(t) = MN\,\mathrm{sech}(Mt), \tag{29}$$

where

$$M = \sqrt{\frac{g_1 L_{\mathrm{Er}}}{\chi d_+^2 - \chi - \eta d_+}}, \tag{30}$$

$$N = \sqrt{\frac{3d_+[4\chi^2 + \eta^2]}{2(L_1 + L_2 + L_{\mathrm{Er}})[\eta\mathcal{D}_i - 2\chi\mathcal{D}_r]}}. \tag{31}$$

Expression (26) is meaningful only if both M and N are real. Indeed, for solution (29) to exist, the inverse M of the pulse length must be real. Therefore, the quantities

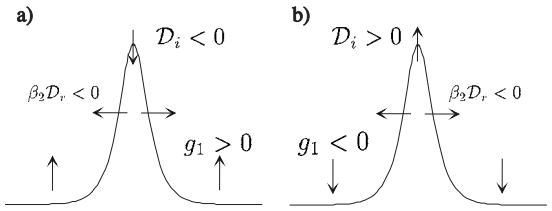

FIG. 2. Schematic representation of the effect of the nonlinear gain $\mathcal{D}_i$ of the excess of linear gain g_1 and of both the dispersion β_2 and the effective self-phase modulation $\mathcal{D}_r$ on a localized pulse.

$(\chi d_+^2 - \chi - \eta d_+)$ and g_1 must be same signs. The stability of the localized solution results from an equilibrium between the excess of linear gain, the quantity $\beta_2\mathcal{D}_r$, and the effective nonlinear gain. Indeed, in the defocusing case where $\beta_2\mathcal{D}_r < 0$, if (i) the excess of linear gain g_1 is negative, (ii) the effective nonlinear gain $\mathcal{D}_i$ is positive, as shown in Fig. 2. Thus, the criterion

$$(\chi d_+^2 - \chi - \eta d_+) < 0 \tag{32}$$

is satisfied, the pulses have a stable shape and arise spontaneously from the background [9]. However, their number tends to increase with the number of round-trips ξ. Inclusion of higher order terms or of gain saturation can definitely stabilize the short pulse solution of Eq. (21). If g_1 is positive and $\mathcal{D}_i$ negative (Fig. 2), the nonconservative effects decrease the amplitude at the top of the pulse, and increase it at the bottom: no stable localized pulse can be formed.

D. Discussion

In the previous section we have derived the stability condition for the cw and the pulsed regime. The expressions take into account the coupling coefficient k, the orientation of the polarizer θ, and the length of the NOLM L_2. In the following, we fix the length L_2 and we vary k from 0 to 1 (excluding $k=0.5$ because for this value losses are infinite: to create an artificial saturable absorber by NOLM it is necessary to use an asymmetrical fiber coupler [13,18]) and θ from 0 to 180°. The range of variation of θ is limited to 180° because the above formulas have this periodicity, and hence also has the laser regime. Results are summarized in a diagram which gives, in the plane (θ,k), the regions of stability of the cw and the mode-locked solutions.

We have first increased L_2 by step of 0.5 m and plotted the corresponding stability diagrams. We have observed that the diagrams are almost periodic versus L_2. The period is about 3.16 m. In the first half period we observe two areas where the mode-lock regime is stable. The first one is located between $\theta=0°$ and $\theta=45°$, and the second one is in the range from $\theta=135°$ to $\theta=180°$. In the second half period, the stable region of the pulse is located between $\theta=45°$ and $\theta=135°$. These results are illustrated in Fig. 3(a) for $L_2=1.5$ m and Fig. 3(b) for $L_2=2$ m. The transition of the stability diagram from the first half period to the second half period is not abrupt. Indeed, the study of the evolution of the stability of the laser regimes versus L_2 reveals that the effect of k on the cartographies is important only for L_2 values

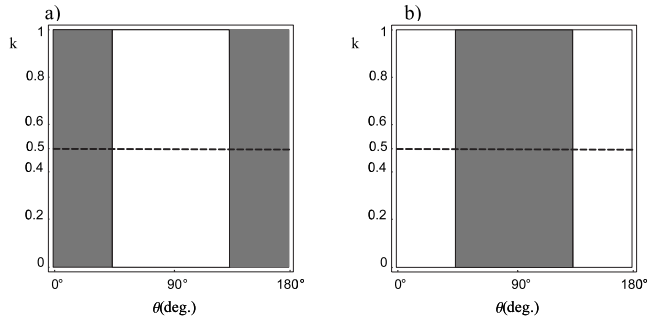

FIG. 3. Stability diagram of the cw and the mode-locked solutions for (a) $L_2=1.5$ m and (b) $L_2=2$ m in the plane (θ,k). The white region corresponds to stable cw operation and unstable mode-locking, the dark gray region corresponds to stable mode-locking operation and unstable cw. On the dotted line $k=0.5$ there is no laser emission.

close to an integer factor of the half period. This is illustrated in Fig. 4 calculated for $L_2=1.57$ m. To confirm these results we have plotted the stability diagram in the plane (θ,L_2) in Fig. 5. The operating regime of the figure-eight laser is almost periodic versus L_2. Indeed, the period and the pattern undergo very little modification.

We observe that as the length L_2 increases up to 32.5 m, the regions of stable pulse narrow and the effect of k increases. The former is due to the effect of dispersion. Indeed, while approaching $L_2=33$ m, the total cavity dispersion approaches the zero net dispersion. This leads to an imbalance between the parameters which stabilize the pulse [19]: the excess of linear gain, the quantity $\beta_2\mathcal{D}_r$, and the effective nonlinear gain. Moreover, the effect of the third order dispersion, which is not accounted for by our model, becomes important. For large values of L_2, a small variation of k induces a great nonlinear phase delay between clockwise and counterclockwise fields in the NOLM. The stability diagram in the plane (θ,k) is represented in Fig. 6 for $L_2=31.5$ m.

Our model is rather than a general one which needs to be adapted to a given configuration. Indeed, we have taken into

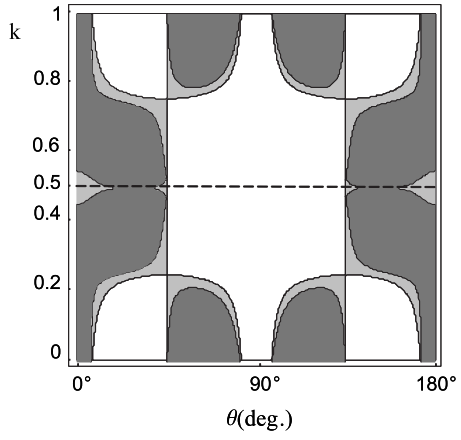

FIG. 4. Stability diagram of the cw and the mode-locked solutions for $L_2=1.57$ m in the plane (θ,k). The colors have the same meaning as in Fig. 3. The light gray corresponds to unstable cw and mode locking.

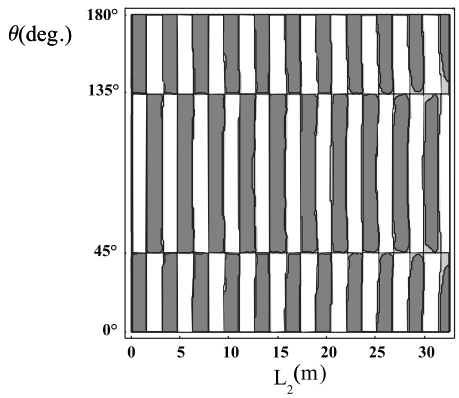

FIG. 5. Stability diagram of the cw and the mode-locked solutions for $k=0.1$ in the plane (θ, L_2). The colors have the same meaning as in Fig. 4.

account all the necessary, but minimum, optical elements required to obtain the mode locking. Practical configurations often include additional optical elements thus rending difficult a direct comparison. However, some of our general results were experimentally demonstrated in the literature: the necessity to use an asymmetrical coupler [18], the dependence of pulse peak power and pulse width versus the length of dispersion-shifted fiber in the NALM [3]. Indeed, the pulse width $1/M$ and the pulse peak power $M\int|a(t)|^2dt$ are sensitive to changes in the GVD and the length of the cavity, in particular the length L_2.

III. ANOMALOUS DISPERSION

A. Solutions and their stability

In this section we investigate a figure-eight laser operating in the anomalous dispersion case. For that we take a length L_2 higher than 33 m and we use the master equation derived in the normal dispersion case. The expression and the criterion of stability of the constant solution are the same as derived in Sec. II.

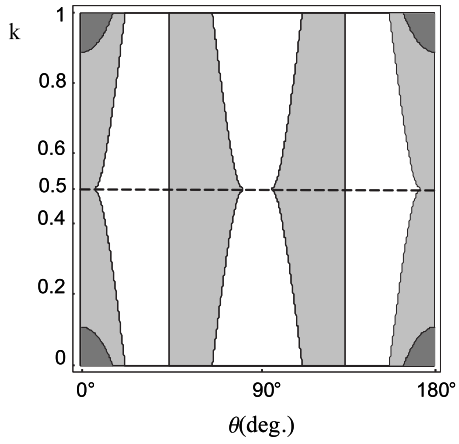

FIG. 6. Stability diagram of the cw and the mode-locked solutions for $L_2=31.5$ m in the plane (θ, k). The colors have the same meaning as in Fig. 4.

In order to study the soliton solution, we use the results of Akhmediev [17]. For that, Eq. (21) is written in the normalized form

$$i\frac{\partial\Psi}{\partial\xi}+\frac{1}{2}\frac{\partial^2\Psi}{\partial\tau^2}+\Psi|\Psi|^2=ig_1\Psi+iD\Psi|\Psi|^2+iR\frac{\partial^2\Psi}{\partial\tau^2}, \tag{33}$$

where

$$\Psi=\sqrt{|\mathcal{D}_r|}\mathrm{F},$$

$$\tau=t\sqrt{(L_1+L_2+L_{\mathrm{Er}})}/\sqrt{|\eta|},$$

$$R=\chi/|\eta|,$$

and

$$D=-\mathcal{D}_i/\mathcal{D}_r.$$

The normalized gain filtering parameter R and the normalized nonlinear gain D are the main parameters of the analysis. They are denoted by β and ϵ, respectively, in the publications by Akhmediev and his co-workers. Numerical computation shows that $\mathcal{D}_r$ is always negative, so that D and $\mathcal{D}_i$ have the same sign.

Mathematically the expression of the soliton solution of Eq. (33) is

$$\Psi=\mathcal{A}(\tau)^{1+id_-}e^{-i\omega_-\xi}, \tag{34}$$

with

$$d_-=\frac{3(1+2DR)-\sqrt{9(1+2DR)^2+8(D-2R)^2}}{2(D-2R)} \tag{35}$$

and

$$\omega_-=\frac{-g_1(1-d_-^2+4Rd_-)}{2(d_--R+Rd_-^2)}. \tag{36}$$

d_- represents the chirp parameter. The amplitude of the pulse writes as

$$\mathcal{A}(\tau)=\mathcal{M}\mathcal{N}\,\mathrm{sech}(\mathcal{M}\tau), \tag{37}$$

where

$$\mathcal{M}=\sqrt{\frac{g_1}{d_--R+Rd_-^2}} \tag{38}$$

and

$$\mathcal{N}=\sqrt{\frac{3d_-(1+4R^2)}{2(2R-D)}}. \tag{39}$$

Akhmediev *et al.* [17] have given the criteria of existence and stability of this solution in the case of positive nonlinear gain D or $\mathcal{D}_i$. They found that the localized solution (34) is stable when the background state is unstable, thus, when the excess of linear gain g_1 is positive. On the other hand, the existence of the soliton is possible if the quantities $(d_--R+Rd_-^2)$ and g_1 have same signs, the stability condition becomes

$$d_- - R + Rd_-^2 > 0. \tag{40}$$

This condition can be written in another way: in the plane (R,D), the solution is stable below the curve

$$D = D_S = R\frac{3\sqrt{1+4R^2}-1}{4+18R^2}, \tag{41}$$

and unstable above this curve. When the nonlinear gain $\mathcal{D}_i$ or D is negative, no such condition is known at this time. The nonzero constant solution is stable in this case for a positive excess of linear gain g_1, allowing to conclude to continuous laser emission. However, a situation where bistability between continuous and mode-locked emission occurs could be envisaged. This would mean that the mode-locking will not be self-starting.

B. Pulse energy

Following the approach developed in Ref. [10], it is possible to extract the soliton energy from the theoretical results. The gain compensating the linear losses can be written as

$$g_0 = \frac{g'}{1+\dfrac{E}{W_S}}, \tag{42}$$

where $g' = 1.26\ \text{m}^{-1}$ is the unsaturated gain, $W_S = 0.1$ pJ the saturation energy, and E the pulse energy. From Eq. (42) and using the expression of g_0 given in the Eq. (16), we can extract the expression of the energy.

We have studied the variation of the pulse energy in the plane (θ,k) and for different lengths L_2. L_2 has been varied from 34 to 100 m with a step of 1 m. The dependence of energy versus L_2 is not very strong because of the smallness of the mode-locking regions. The most important result from our analytical simulation is that the zones of the most energetic pulses are small. An example of cartography is represented in Fig. 7 for $L_2 = 39$ m. The energetic solitons are obtained with high asymmetrical coupler. In the vicinity of $k = 0.5$, the pulses are weakly energetic. With the parameters used, the laser delivers pulse energies up to 10 pJ. To obtain these energies in experiments, it is necessary that the orientation of the polarizer and the coupling coefficient are adjusted with high precisions because the regions where the pulses are energetic are narrow.

C. Pulse duration

In our model the stable state of the soliton is reached after several round-trips in the cavity. It takes the shape of a hyperbolic secant. The pulse width in normalized units is determined by

$$\tau_0 = \frac{1}{\mathcal{M}}. \tag{43}$$

Because of the dependence of $\mathcal{M}$ on the parameters of the figure-eight laser, the duration τ_0 depends on the coupling coefficient k, the orientation of the polarizer and the length of the nonlinear optical loop. To study the influence of these parameters on τ_0, it is necessary to express $\mathcal{M}$ as a function of parameters other than g_1. Indeed, the latter is self-adjusted to a value which is not known in our calculation. For that we use the pulse energy $E = \int |F|^2 dt$ to find the expression of $\mathcal{M}$. After calculation we obtain

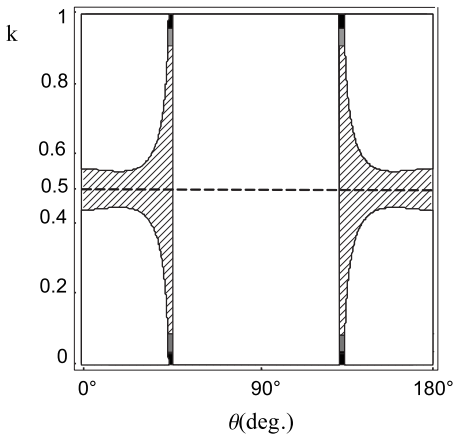

FIG. 7. Evolution of the pulse energy in the plane (θ,k) at $L_2 = 39$ m. In the black region the energy is above 10 pJ, in the gray region the energy is between 5 and 10 pJ and in the hatched region the energy is below 5 pJ. In the white region, either the pulse are unstable, or their stability is not determined and continuous emission occurs. On the dotted line $k = 0.5$ there is no laser emission.

$$E = \frac{2\sqrt{|\eta|}\mathcal{M}\mathcal{N}^2}{\sqrt{L_1+L_2+L_{\text{Er}}}|\mathcal{D}_r|}. \tag{44}$$

On the other hand, we have the expression of E given by the formula (42) and $\mathcal{N}$ by (39), we can deduce the expression of the soliton duration t_0 (in ps), as

$$t_0 = \frac{\tau_0\sqrt{|\eta|}}{L_1+L_2+L_{\text{Er}}} = \frac{2|\eta|\mathcal{N}^2}{|\mathcal{D}_r|(L_1+L_2+L_{\text{Er}})\left(\dfrac{g'}{g_0}-1\right)W_S}, \tag{45}$$

where W_S is in pJ.

The expression of the pulse duration (45) shows that the pulse width is affected by the pulse energy $(g'/g_0 - 1)W_S$, the total dispersion in the cavity η and nonlinear effects corresponding to the effective self-phase modulation $\mathcal{D}_r$ and the effective nonlinear gain or absorption $\mathcal{D}_i$. As a consequence, the soliton duration undergoes large variations as k, θ, and L_2 vary.

As it has been done for the study of energy, we explore the dependence of the pulse duration in the plane (θ,k) versus the length L_2 of the NOLM. L_2 has been varied between 34 m and 100 m by a step of 1 m. An example of cartography is represented in Fig. 8 for $L_2 = 39$ m. A feature common to all diagrams is that the regions of ultrashort pulses are small.

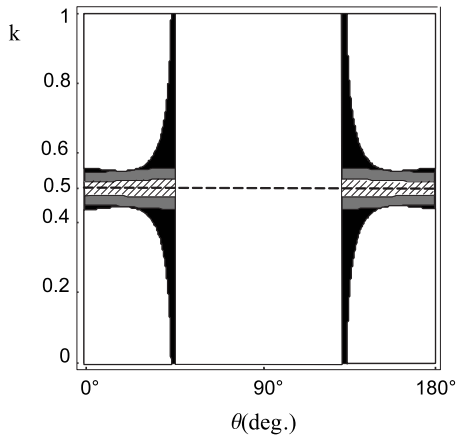

FIG. 8. Evolution of the pulse duration in the plane (θ,k) at $L_2=39$ m. In the hatched region the duration is above 1 ps, in the gray region it is between 0.5 and 1 ps and in the black region below 0.5 ps. The white region and the dotted line have the same meanings as in Fig. 7.

In addition, the broadest solitons are localized around $k=0.5$. The model predicts pulses widths shorter than 500 fs. From the experimental point of view, the production of ultrashort pulses from figure-eight laser is difficult because it is necessary to optimize with a high degree of precision the parameters of the cavity, in particular the orientation of the polarizer, the coupling coefficient and the length of the nonlinear optical loop mirror. This experimental result is reported by Agrawal in Ref. [18]: it is generally difficult to generate pulses shorter than 100 fs.

IV. CONCLUSION

We have given through this study a fully analytical model to describe a figure-eight passively mode-locked all fiber laser. We have derived a master equation valid for normal and anomalous dispersion regimes. In both cases, the master equation is of CGL type. The coefficients of the equation have an explicit dependence on the parameters of figure-eight laser, in particular on the orientation of the polarizer, the coupling coefficient and the length of the nonlinear optical loop mirror.

In the normal dispersion case we have investigated the existence and the stability of the cw and mode-locking operations. We have given the regions where the pulses are stable in the plane (θ,k). The influence of the length of the NOLM was also studied. In the anomalous dispersion regime we have investigated the soliton characteristics. In the plane (θ,k), the model predicts small regions where the pulses are simultaneously energetic and ultrashort.

APPENDIX

In this appendix, we give the results of the analytical resolution of the propagation equations, for each piece of fiber.

1. Propagation along the standard fiber

We denote by $[u(0),v(0)]$ the electric-field components at the entrance of the piece of the standard fiber. After propagation over a distance L_1 they become $[u(L_1),v(L_1)]$, with the expressions

$$u(L_1) = u(0)e^{-in_sL_1} + \epsilon\left\{-\frac{i\beta_2^s}{2}L_1\frac{\partial^2 u(0)}{\partial t^2} + i\gamma L_1[u(0)|u(0)|^2 + Au(0)|v(0)|^2] + \frac{\gamma B}{4n_s}(e^{4in_sL_1}-1)v(0)^2u(0)^*\right\}e^{-in_sL_1} + O(\epsilon^2), \tag{A1}$$

$$v(L_1) = v(0)e^{in_sL_1} + \epsilon\left\{-\frac{i\beta_2^s}{2}L_1\frac{\partial^2 v(0)}{\partial t^2} + i\gamma L_1[v(0)|v(0)|^2 + Av(0)|u(0)|^2] - \frac{\gamma B}{4n_s}(e^{-4in_sL_1}-1)u(0)^2v(0)^*\right\}e^{in_sL_1} + O(\epsilon^2). \tag{A2}$$

2. The fiber coupler and the NOLM

The expressions of the electric field components after propagation in either direction in the NOLM are as follows:

$$E_{+u}(L_2) = \sqrt{k}u(L_1)e^{-in_sL_2} + \epsilon\left\{\sqrt{k}L_2\left(\frac{-i\beta_2^s}{2}\right)\frac{\partial^2 u(L_1)}{\partial t^2} + i\gamma L_2k^{3/2}[u(L_1)|u(L_1)|^2 + Au(L_1)|v(L_1)|^2] + \frac{B\gamma k^{3/2}}{4n_s}(e^{4in_sL_2}-1)v(L_1)^2u(L_1)^*\right\}e^{-in_sL_2} + O(\epsilon^2), \tag{A3}$$

$$E_{+v}(L_2) = \sqrt{k}v(L_1)e^{in_sL_2} + \epsilon\left\{\sqrt{k}L_2\left(\frac{-i\beta_2^s}{2}\right)\frac{\partial^2 v(L_1)}{\partial t^2} + i\gamma L_2k^{3/2}[v(L_1)|v(L_1)|^2 + Av(L_1)|u(L_1)|^2] - \frac{B\gamma k^{3/2}}{4n_s}(e^{-4in_sL_2}-1)u(L_1)^2v(L_1)^*\right\}e^{in_sL_2} + O(\epsilon^2), \tag{A4}$$

$$E_{-u}(L_2) = i\sqrt{1-k}u(L_1)e^{-in_sL_2} + \epsilon\left\{\frac{\sqrt{1-k}}{2}L_2\beta_2^s\frac{\partial^2 u(L_1)}{\partial t^2} - \gamma L_2(1-k)^{3/2}[u(L_1)|u(L_1)|^2 + Au(L_1)|v(L_1)|^2] + \frac{i\gamma B(1-k)^{3/2}}{4n_s}(e^{4in_sL_2}-1)v(L_1)^2u(L_1)^*\right\}e^{-in_sL_2} + O(\epsilon^2), \tag{A5}$$

$$E_{-v}(L_2) = i\sqrt{1-k}v(L_1)e^{in_sL_2} + \epsilon\left\{\frac{\sqrt{1-k}}{2}L_2\beta_2^s\frac{\partial^2 v(L_1)}{\partial t^2} - \gamma L_2(1-k)^{3/2}[v(L_1)|v(L_1)|^2 + Av(L_1)|u(L_1)|^2] - \frac{i\gamma B(1-k)^{3/2}}{4n_s}(e^{-4in_sL_2}-1)u(L_1)^2v(L_1)^*\right\}e^{in_sL_2} + O(\epsilon^2). \quad \text{(A6)}$$

3. Propagation along the erbium-doped fiber

The expressions of the electric field components $E_{tv}(L_{\mathrm{Er}})$, $E_{tv}(L_{\mathrm{Er}})$ after propagation in the doped fiber are

$$E_{tu}(L_{\mathrm{Er}}) = E_{tu}e^{(g-in_{\mathrm{Er}})L_{\mathrm{Er}}} + \epsilon\left\{L_{\mathrm{Er}}\left(\rho - \frac{i\beta_2^{\mathrm{Er}}}{2}\right)\frac{\partial^2 E_{tu}}{\partial t^2} + i\gamma(E_{tu}|\ E_{tu})|^2 + AE_{tu}|E_{tv}|^2)\frac{e^{2gL_{\mathrm{Er}}}-1}{2g} + i\gamma BE_{tv}^2E_{tu}^*\frac{e^{(2g+4in_{\mathrm{Er}})L_{\mathrm{Er}}}-1}{(2g+4in_{\mathrm{Er}})}\right\}e^{(g-in_{\mathrm{Er}})L_{\mathrm{Er}}} + O(\epsilon^2), \quad \text{(A7)}$$

$$E_{tv}(L_{\mathrm{Er}}) = E_{tv}e^{(g+in_{\mathrm{Er}})L_{\mathrm{Er}}} + \epsilon\left\{L_{\mathrm{Er}}\left(\rho - \frac{i\beta_2^{\mathrm{Er}}}{2}\right)\frac{\partial^2 E_{tv}}{\partial t^2} + i\gamma[E_{tv}|\ E_{tv})|^2 + AE_{tv}|E_{tu}|^2]\frac{e^{2gL_{\mathrm{Er}}}-1}{2g} + i\gamma BE_{tu}^2E_{tv}^*\frac{e^{(2g-4in_{\mathrm{Er}})L_{\mathrm{Er}}}-1}{(2g-4in_{\mathrm{Er}})}\right\}e^{(g+in_{\mathrm{Er}})L_{\mathrm{Er}}} + O(\epsilon^2). \quad \text{(A8)}$$

[1] J. Goodberlet, J. Wang, J. G. Fujimoto, and P. A. Schulz, Opt. Lett. **14**, 1125 (1989).
[2] V. J. Matsas, T. P. Newson, D. J. Richardson, and D. N. Payne, Electron. Lett. **28**, 1391 (1992).
[3] T. O. Tsun, M. K. Islam, and P. L. Chu, Opt. Commun. **141**, 65 (1997).
[4] M. J. Guy, D. U. Noske, A. Boskovic, and J. R. Taylor, Opt. Lett. **19**, 828 (1994).
[5] E. A. Kuzin, B. Ibarra Escamilla, D. E. Garcia-Gomez, and J. W. Hauss, Opt. Lett. **26**, 1559 (2001).
[6] A. V. Avdokhin, S. V. Popov, and J. R. Taylor, Opt. Express **11**, 265 (2003).
[7] Y. Zhao, S. Min, H. Wang, and S. Fleming, Opt. Express **14**, 10475 (2006).
[8] J. Theimer and J. W. Haus, J. Mod. Opt. **44**, 919 (1997).
[9] H. Leblond, M. Salhi, A. Hideur, T. Chartier, M. Brunel, and F. Sanchez, Phys. Rev. A **65**, 063811 (2002).
[10] M. Salhi, H. Leblond, and F. Sanchez, Phys. Rev. A **67**, 013802 (2003).
[11] M. Salhi, H. Leblond, and F. Sanchez, Phys. Rev. A **68**, 033815 (2003).
[12] G. P. Agrawal, *Nonlinear Fiber Optics*, 2nd ed. (Academic Press, New York, 1995).
[13] A. Haboucha, M. Salhi, A. Komarov, H. Leblond, and F. Sanchez, J. Nonlinear Opt. Phys. Mater. **15**, 157 (2006).
[14] A. D. Kim, J. N. Kutz, and D. J. Muraki, IEEE J. Quantum Electron. **36**, 465 (2000).
[15] T. Taniuti and C.-C. Wei, J. Math. Phys. **14**, 1389 (1973).
[16] N. J. Doran and D. Wood, Opt. Lett. **13**, 56 (1988).
[17] N. N. Akhmediev and A. Ankiewicz, *Solitons, Nonlinear Pulses and Beams* (Chapman and Hall, London, 1997).
[18] G. P. Agrawal, *Applications of Nonlinear Fiber Optics* (Academic Press, New York, 2001).
[19] B. Ortaç, A. Hideur, M. Brunel, T. Chartier, M. Salhi, H. Leblond, and F. Sanchez, Appl. Phys. B: Lasers Opt. **77**, 589 (2003).